Chemistry–A European Journal
Research Article
doi.org/10.1002/chem.202104314
Chemistry Europe
European Chemical Societies Publishing
www.chemeurj.org

Quantitative Assessment of Ligand Substituent Effects on σ- and π-Contributions to Fe–N Bonds in Spin Crossover Fe^{II} Complexes

Luca Bondì,[a, b] Anna L. Garden,[a] Federico Totti,*[b] Paul Jerabek,*[c] and Sally Brooker*[a]

Abstract: The effect of *para*-substituent **X** on the electronic structure of sixteen tridentate 4-**X**-(2,6-di(pyrazol-1-yl))-pyridine (**bpp**^{X}) ligands and the corresponding solution spin crossover $[Fe^{II}(\mathbf{bpp}^{X})_2]^{2+}$ complexes is analysed further, to supply quantitative insights into the effect of **X** on the σ-donor and π-acceptor character of the Fe-$\mathbf{N_A}$(pyridine) bonds. EDA-NOCV on the sixteen *LS* complexes revealed that neither $\Delta E_{orb,\sigma+\pi}$ ($R^2 = 0.48$) nor $\Delta E_{orb,\pi}$ ($R^2 = 0.31$) correlated with the experimental solution $T_{1/2}$ values (which are expected to reflect the ligand field imposed on the iron centre), but that $\Delta E_{orb,\sigma}$ correlates well ($R^2 = 0.82$) and implies that as **X** changes from **EDG**→**EWG** (Electron Donating to Withdrawing Group), the ligand becomes a better σ-donor. This counter-intuitive result was further probed by Mulliken analysis of the $\mathbf{N_A}$ atomic orbitals: $\mathbf{N_A}(p_x)$ involved in the Fe–N σ-bond vs. the perpendicular $\mathbf{N_A}(p_z)$ employed in the ligand aromatic π-system. As **X** changes **EDG**→**EWG**, the electron population on $\mathbf{N_A}(p_z)$ decreases, making it a better π-acceptor, whilst that in $\mathbf{N_A}(p_x)$ increases, making it a better σ-bond donor; both increase ligand field, and $T_{1/2}$ as observed. In 2016, Halcrow, Deeth and co-workers proposed an intuitively reasonable explanation of the effect of the *para*-**X** substituents on the $T_{1/2}$ values in this family of complexes, consistent with the calculated MO energy levels, that M→L π-backdonation dominates in these M–L bonds. Here the quantitative EDA-NOCV analysis of the M–L bond contributions provides a more complete, coherent and detailed picture of the relative impact of M–L σ-versus π-bonding in determining the observed $T_{1/2}$, refining the earlier interpretation and revealing the importance of the σ-bonding. Furthermore, our results are in perfect agreement with the ΔE(HS-LS) vs. σ_p^+(X) correlation reported in their work.

Introduction

Predictable fine tuning of the electronic structure of metal complexes is highly desirable, not least in order to optimise them for use in practical applications, such as molecular electronics,[1] emissive devices,[2] catalysis[3] or photovoltaics.[4] The choice of substituent **X** present in a 5- or 6-membered aromatic ring is an important and frequently employed tool for fine-tuning the electronic structure of organic and inorganic compounds.

Substituent effects are commonly parameterised using the Hammett constant (σ(**X**) or σ^+(**X**)): σ(**X**) comes from acid/base dissociation of *para/meta* substituted benzoic acids, whereas σ^+(**X**) comes from nucleophilic substitution at the carbonyl carbon in *para/meta* substituted benzoic acid derivatives and better reflects resonance effects.[5–6] The Hammett parameters for *para*-**X** substituents, σ_p(**X**) and σ_p^+(**X**), range from those for very Electron Donating Groups (**EDG**, **X** = **NMe$_2$**; $\sigma_p = -0.83$, $\sigma_p^+ = -1.70$) to those for very Electron Withdrawing Groups (**EWG**, **X** = **NO$_2$**; $\sigma_p = 0.78$, $\sigma_p^+ = 0.79$). As expected, *meta*-**Y** substituents have far less electronic impact so have a much narrower range of σ_m^+(**Y**) values, from the lowest **EDG** (**Y** = **Me**; $\sigma_m = \sigma_m^+ = -0.07$) to the highest **EWG** (**Y** = **NO$_2$**; $\sigma_m = 0.71$, $\sigma_m^+ = 0.67$).[7]

Many studies have tried, with varying success, to rationalise how ligand substituent modifications affect key properties such as the molecular orbital (*MO*) energies,[8] redox potentials[9] as well as spin crossover (*SCO*) switching temperatures.[8b,10] The focus herein is on *SCO*, which occurs when the metal ion **M** (usually $3d^4$ to $3d^7$ electronic configuration in octahedral geometry) can be switched between the high spin (*HS*) and low spin (*LS*) states through a trigger stimulus such as temperature, pressure, host-guest interaction, external magnetic field or light irradiation.[11] Systems showing thermal *SCO* in the solution phase are particularly suitable candidates for monitoring the **X**

[a] Dr. L. Bondì, Dr. A. L. Garden, Prof. S. Brooker
Department of Chemistry
MacDiarmid Institute of Advanced Materials and Nanotechnology
University of Otago
PO Box 56, Dunedin 9054 (New Zealand)
E-mail: sbrooker@chemistry.otago.ac.nz

[b] Dr. L. Bondì, Prof. F. Totti
Department of Chemistry
'Ugo Schiff' and INSTM Research Unit
University of Florence
50019 Sesto Fiorentino (Italy)
E-mail: federico.totti@unifi.it

[c] Dr. P. Jerabek
Institute of Hydrogen Technology
Helmholtz-Zentrum Hereon
Max-Planck-Straße 1, 21502 Geesthacht (Germany)
E-mail: paul.jerabek@hereon.de

Supporting information for this article is available on the WWW under https://doi.org/10.1002/chem.202104314

(or **Y**) effects on the **M**–**L** bond, as they are not complicated by the effects of crystal packing or solvatomorphs;[12] so, providing speciation is not a problem, variations in the ligand field strength due to **X** (or **Y**) substituent, are more clearly observed in solution[8b,10, 13] than in the solid state *SCO*.[14] For thermal *SCO*, the switching temperature $T_{1/2}$ (the temperature at which there is a *50:50* ratio of *HS:LS*) is determined in order to monitor these variations.[8b,13, 15]

A landmark study on the effects of *para*-**X** (and *meta*-**Y**) substituents on solution *SCO* $T_{1/2}$ values was reported by Deeth, Halcrow and co-workers in 2016,[8b] and this was followed up with further papers by them in in 2018[16] and 2019.[12] They focused on the largest known family of solution *SCO* active complexes, $[Fe^{II}(\mathbf{bpp}^{X,Y})_2]^{2+}$ (where $\mathbf{bpp}^{X,Y}$ = 4-**X**-2,6-di(pyrazol-3-**Y**-1-yl)-pyridine; Figure 1 shows only the 16 complexes focused on herein, for which the '*meta*' pyrazole substituent is held constant as **Y** = **H** whilst the para substituent **X** is varied), which had been prepared and studied by various authors across the years.[14g,17] In their landmark paper[8b] they found a strong positive correlation (R^2 = 0.92) of σ_p^+(**X**) vs. $T_{1/2}$ and as expected a weaker, but also negative, correlation (R^2 = 0.61) of σ_m(**Y**) vs. $T_{1/2}$. They also found, by using quantum-chemical calculation based on Density Functional Theory (*DFT*), that (a) the difference between the *HS* and *LS* total energies, ΔE_{rel}*(HS-LS)*, correlated strongly with σ_p^+(**X**) (R^2 = 0.89) and less strongly with σ_m(**Y**) (R^2 = 0.67); and (b) σ_p^+(**X**) and σ_m(**Y**) correlated extremely well (R^2 = 0.93–0.99) with the average energy levels, $<E(t_{2g})>$ and $<E(e_g)>$, calculated for *LS* $[Fe^{II}(\mathbf{bpp}^{X,H})_2]^{2+}$ (R^2 = 0.94–0.93) and *LS* $[Fe^{II}(\mathbf{bpp}^{H,Y})_2]^{2+}$ (R^2 = 0.99–0.98). They concluded that there is a "fine balance between opposing M–L σ- and π-bonding effects", and that for the present family: (a) Fe→N π-backbonding effects must be dominating for *para*-**X** substituents because **EDG**→**EWG** increases the observed $T_{1/2}$, the rationale being that this is expected to decrease the energy of the ligand π* *MO*s and therefore increase the **M**→**L** π-backbonding, increasing the ligand field strength and $T_{1/2}$, whereas (b) Fe ← N σ-bonding effects must be dominating for the *meta*-**Y** substituents as **EDG**→**EWG** decreases the observed $T_{1/2}$, the rationale being that this is expected to decrease the energy of the lone pairs, making them poorer **M**←**L** σ-donors, decreasing the ligand field strength and hence also the $T_{1/2}$.[8b] The quantitative EDA-NOCV analysis carried out herein enables us to refine this interpretation, and reveals the importance of the σ-bonding (see later).

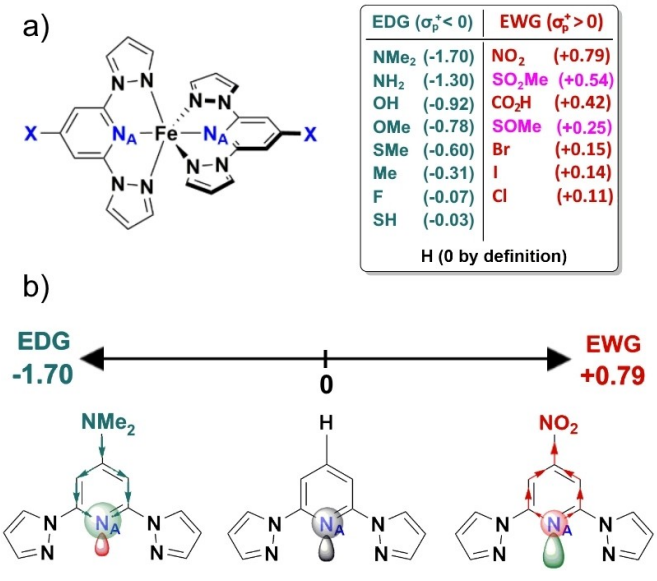

Figure 1. Representations of (a) the members of the $[Fe^{II}(\mathbf{bpp}^{X})_2]^{2+}$ family and the Hammett constants (σ_p^+(**X**)) for the para-**X** substituents employed; (b) electrostatic effects on the pyridine nitrogen donor atom, $\mathbf{N_A}$, by either (left) electron donating group (**EDG**) or (right) electron withdrawing group (**EWG**) substituent in $[Fe^{II}(\mathbf{bpp}^{X})_2]^{2+}$. Pink text for the two **X** for which σ_p^+ is not experimentally known but is estimated from the correlations presented herein (Table S12–S13).

The present study was motivated by the above findings[8b] and by the promise shown in our first use of *EDA-NOCV* theory, which is a combination of *EDA* (Energy Decomposition Analysis),[18] with the *NOCV* (Natural Orbitals for Chemical Valence)[19] concept that provides quantitative and chemically intuitive analysis of bonding – to a solution *SCO* system, specifically a family of five $[Fe^{II}(\boldsymbol{L}^{azine})_2(NCBH_3)_2]$ complexes.[20] The latter study[20] first established a new and general fragmentation protocol ($\mathbf{M}+\mathbf{L_x}$) for computationally evaluating **M**–**L** bond strength in any kind of metal complex, diamagnetic or paramagnetic. Such corrected approach overcomes limits of partial $\mathbf{ML_6}$ fragmentations ($\mathbf{ML_n}+\mathbf{L_{x\text{-}n}}$), proposing a common ground state (the 'naked' metal ion **M**) to treat any complex independently from the ligand coordination pocket. Then this protocol was applied to the family of five $[Fe^{II}(\boldsymbol{L}^{azine})_2(NCBH_3)_2]$ complexes, revealing a strong correlation (R^2 = 0.99) between $\Delta E_{orb,\sigma+\pi}$ for the Fe–N bonds and the experimental $T_{1/2}$ for solution *SCO*.

Another important study aimed at improved our detailed understanding of σ- and π-tuning operated by *para*-**X**-substituents was reported by Ashley and Jakubikova in 2018.[21a] They carried out a DFT and EDA-NOCV study on a family of *LS* iron(II) complexes of para-**X** substituted bipyridine ligands, $[Fe(\mathbf{bpy}^{X})_3]^{2+}$, and found that the ligands show both π-acceptor and π-donor character, but recommend that the results should be taken with caution until they can be experimentally verified in some way. They also commented that use of substituents **X** should be a good way to make small adjustments of ligand field, and hence precisely tune the $T_{1/2}$ in an *SCO* complex (without pushing the complex either LS or HS). Clearly $T_{1/2}$ is an experimental outcome that can be used to validate theoretical predictions of how a change in **X** will tune the ligand field. Such a validation of in silico predictions, pre-synthesis, is key as it will enable future synthetic efforts to focus on only preparing the best candidate for a desired $T_{1/2}$ or indeed spin state. Given that spin state is key to properties and function, including catalytic, the importance of this is clear.[21b]

Herein, EDA-NOCV methodology is applied for only the second time to an *SCO* system – in this case to the large family of sixteen *para*-**X** substituted $[Fe^{II}(\mathbf{bpp}^{X})_2]^{2+}$ complexes (Figure 1), in order to quantify the relative importance of the σ- and π-contributions to the **M**–**L** bonds as **X** is varied as **EDG**→**EWG**, and look for correlations between the obtained parameters and

the experimentally observed $T_{1/2}$ values. As this led to unexpected results, an in-depth Mulliken charge analysis[22] of the N-donor atomic orbitals (*AOs*) population was also performed, to provide further insights and explanations.

Finally, the correlations obtained are employed (a) to test how well the known Hammett σ_p(**X**) parameters for **X** = **SOMe** and **SO_2Me** were reproduced, then (b) to predict approximate values for the unknown σ_p^+(**X**) for these two substituents **X**.

Introduction to EDA-NOCV

The EDA-NOCV[23] method involves a "classical" EDA,[18] followed by a NOCV procedure.[19] In this work, it is used to single out and quantify the various energy contributions to **M**–**L** bonding. After geometry optimisation, the compound is formally separated into two or more non-interacting fragments, and the intrinsic, instantaneous interaction energy ΔE_{int} of the bonds formed between the fragments in the frozen (unrelaxed) geometry of the molecule is then assessed (Eq. (1)) in a stepwise fashion.[24] The general fragmentation that we developed and validated in a previous study[20] is employed herein (fragmentation **5** in ref;[20] Figure S1): fragment 1 (corrected) = **Fe^{II}** and fragment 2 = **L** (herein both tridentate **bpp^X** ligands).

$$\Delta E_{int} = \Delta E_{elstat} + \Delta E_{Pauli} + \Delta E_{orb} + \Delta E_{disp} \quad (1)$$

Where: ΔE_{elstat} is the electrostatic interaction (usually negative/attractive), ΔE_{Pauli} is the Pauli repulsion (repulsive/positive), ΔE_{orb} is the orbital interaction (attractive/negative; see also Equation (2), below), and ΔE_{disp} is the dispersion term (attractive/negative) accounting for long-range interaction.[25]

Subsequently, NOCV analysis decomposes ΔE_{orb} (Eq. (2)) into several contributions, reflecting electron flows (i.e. deformation densities $\Delta\rho_i$) between (a) two *MOs* on different fragments to give the individual orbital contributions to the σ, π and δ bonds formed ($\Delta E_{orb,i}$, $i = \sigma, \pi, \delta$; identified by visual inspection of $\Delta\rho_i$)[19a,26] and (b) two *MOs* on the same fragment to give the polarization term ($\Delta E_{orb,pol}$).

$$\Delta E_{orb} = \Delta E_{orb,\sigma} + \Delta E_{orb,\pi} + \Delta E_{orb,pol} + \Delta E_{orb,rest} \quad (2)$$

Information about the magnitude of the charge flow is given via the corresponding eigenvalues.[27] Of the many contributions to ΔE_{orb}, those of key importance in octahedral transition metal complexes are:[28] six σ-type interactions ($\Delta E_{orb,\sigma}$) between the **M** *AOs* (d_{x2-y2}, d_{z2}, p_x, p_y, p_z and *s* orbitals) and the *MOs* with the corresponding symmetry in the **L_6** fragment, plus three π-type interactions ($\Delta E_{orb,\pi}$) between the remaining **M** *AOs* (d_{xy}, d_{xz}, d_{yz} orbitals) and the **L_6** *MOs* of appropriate symmetry.

Note that the development and validation of this general fragmentation method (**M** + **6 L**), for dia- and para-magnetic complexes and the application of it to *SCO* complexes for the first time in Ref. [20], and again herein, opens the door quantifying the nature of **M**–**L** bonding in more families of *SCO* complexes (in which the ligand field strength is very delicately poised) and we expect the resulting findings will continue to be revelatory.

Results and Discussion

DFT optimisation of $[Fe^{II}(bpp^X)_2]^{2+}$ (LS and HS)

The geometry optimisation computational protocol employed for the sixteen *LS* and sixteen *HS* $[Fe^{II}(\mathbf{bpp^X})_2]^{2+}$ complexes was chosen based on the functional screening we performed previously.[20] The same computational protocol was applied to all of the candidates, in the same CPCM solvent, acetone, albeit the *LS* forms of the **X** = **NMe_2** or **NH_2** complexes were not observed experimentally. Calculating the Root-Mean-Square-Deviation (*RMSD*) of each atomic position (Eq. S1) in the structures of these $[Fe^{II}(\mathbf{bpp^X})_2]^{2+}$ complexes from that of the respective *LS* or *HS* state of the **X** = **H** parent complex, $[Fe^{II}(\mathbf{bpp^H})_2]^{2+}$, confirmed that the variation of the *para*-substituent **X** causes no significant deviations (*RMSD* < 0.01 Å in all cases, Table S1). The six, out of the sixteen $[Fe^{II}(\mathbf{bpp^X})_2]^{2+}$ complexes, where the experimental $T_{1/2}$ values were measured in nitromethane solvent (Table S1) were subjected to a geometry re-optimisation, and then to a *RMSD* evaluation between the final geometries calculated in acetone vs. nitromethane. Again, the *RMSD* for each atomic position confirmed that, as expected, changing the dielectric constant in the CPCM model,[29] from acetone to nitromethane, has a negligible effect on the optimised structures obtained in these two different solvents (*RMSD* < 0.01 Å in all cases, Table S1).

EDA analysis of effects of X in $[Fe^{II}(bpp^X)_2]^{2+}$ (LS and HS)

EDA,[18] using the previously established optimal fragmentation **5 e** (**M** + **L_6**)[20] (Table S2, see Computational Details section below for details), were performed on the sixteen *HS* and sixteen *LS* $[Fe^{II}(\mathbf{bpp^X})_2]^{2+}$ complexes (Figure 1). This quantified the overall interaction energy, ΔE_{int}, which accounts for the strength of the binding by the coordination sphere onto the iron(II) centre. The ΔE_{int} contribution for *HS* was half that for *LS* $[Fe^{II}(\mathbf{bpp^X})_2]^{2+}$ complexes (Table 1).

This is consistent with the *HS* state being less enthalpically stable than the *LS* state; note these results are obtained at 0 K. Furthermore, as σ_p^+(**X**) increases (**EDG**→**EWG, NMe_2**→**NO_2**), the stabilising energy ΔE_{int} drops in all cases: from about −250 to −200 kcal/mol for the *LS* complexes (**NMe_2**→**NO_2**) and from −120 to −70 kcal/mol (**NMe_2**→**NO_2**) for the *HS* complexes (Figure 2, Tables 1, 2). In the detailed analysis of the various energetic contributions to the ΔE_{int} term, the ΔE_{elstat} term – which accounts for the *ionic* bonding between the fragments – is observed to correlate well with σ_p^+(**X**) for *LS* $[Fe^{II}(\mathbf{bpp^X})_2]^{2+}$ ($R^2 = 0.89$, Table S3, Figure S2) and moderately well for *HS* $[Fe^{II}(\mathbf{bpp^X})_2]^{2+}$ ($R^2 = 0.73$, Table S4 and Figure S3). In both cases, this behaviour can be understood as follows: as **X** becomes more electron poor (σ_p^+ increases) it drains more electron density away from the coordinating nitrogen (Figure 1),

Table 1. EDA results (frag. **5e**) for the sixteen *LS* and *HS* $[Fe(\mathbf{bpp^X})_2]^{2+}$ complexes: all energies are reported in kcal/mol (Note: 1 *eV* = 23 kcal/mol = 8100 cm^{-1}). Results are presented in order of increasing Hammett parameter (σ_p^+). *Values estimated in this study.

X	$T_{1/2}$	σ_p^+	State	ΔE_{int}	ΔE_{elstat}	ΔE_{orb}
NMe_2	*HS*	−1.70	*LS*	−255.0	−413.8	−305.5
			HS	−120.1	−330.6	−503.9
NH_2	*HS*	−1.30	*LS*	−246.7	−409.4	−309.1
			HS	−113.0	−338.2	−409.4
OH	164	−0.92	*LS*	−232.0	−396.2	−307.7
			HS	−98.1	−325.0	−499.5
OMe	158	−0.78	*LS*	−238.9	−401.2	−310.6
			HS	−104.0	−328.7	−501.6
SMe	194	−0.60	*LS*	−239.6	−397.1	−310.6
			HS	−104.4	−326.5	−507.0
Me	216	−0.31	*LS*	−235.6	−397.9	−306.7
			HS	−101.5	−314.3	−502.8
F	215	−0.31	*LS*	−219.5	−385.0	−296.9
			HS	−83.0	−302.9	−499.3
SH	246	−0.03	*LS*	−231.6	−390.7	−314.0
			HS	−98.5	−320.1	−505.6
H	248	0.00	*LS*	−229.1	−393.7	−296.6
			HS	−89.9	−310.7	−501.3
Cl	226	+0.11	*LS*	−221.7	−383.1	−311.8
			HS	−88.2	−312.4	−504.0
I	236	+0.14	*LS*	−224.5	−382.5	−304.1
			HS	−86.9	−300.5	−508.4
Br	234	+0.15	*LS*	−222.9	−383.1	−301.8
			HS	−85.5	−301.1	−505.6
CO_2H	281	+0.42	*LS*	−223.7	−383.4	−314.2
			HS	−89.0	−313.2	−508.3
NO_2	309	+0.79	*LS*	−205.7	−365.4	−508.7
			HS	−71.6	−296.6	−314.9
SOMe*	284	+0.25*	*LS*	−224.4	−368.0	−515.0
			HS	−81.0	−300.8	−305.5
SO_2Me*	294	+0.54*	*LS*	−215.4	−359.1	−515.8
			HS	−90.1	−303.2	−314.8

decreasing the favourable electrostatic interactions with the Fe^{II} ion (Tables S3-S4).

From $\mathbf{X = NMe_2}$ to $\mathbf{X = NO_2}$, ΔE_{elstat} decreases by just −60 kcal/mol (+15%) in the *LS* $[Fe^{II}(\mathbf{bpp^X})_2]^{2+}$ and decreasing by just −35 kcal/mol (+12%) in the *HS* $[Fe^{II}(\mathbf{bpp^X})_2]^{2+}$ complexes. In contrast, the ΔE_{orb} interaction, which accounts for the covalent bonding between the fragments, remains almost constant across the whole range of σ_p^+ values: from $\mathbf{X = NMe_2}$ to $\mathbf{X = NO_2}$, ΔE_{orb} increases by just +20 kcal/mol (+3.5%) in the *LS* $[Fe^{II}(\mathbf{bpp^X})_2]^{2+}$ and decreased by just −5 kcal/mol (−1.5%) in the *HS* $[Fe^{II}(\mathbf{bpp^X})_2]^{2+}$ complexes. Comparing these *EDA* results with those for the $[Fe^{II}(\mathbf{L^{azine}})_2(NCBH_3)_2]$ family ($\boldsymbol{L^{azine}}$ = 3-(2-**azinyl**)-4-tolyl-5-phenyl-1,2,4-triazole; (Table 2),[20] few differences can be grouped up. The ΔE_{int} energies for the $[Fe^{II}(\boldsymbol{L^{azine}})_2(NCBH_3)_2]$ family are twice the size of those for the $[Fe^{II}(\mathbf{bpp^X})_2]^{2+}$ family,[20] but yet, the ΔE_{orb} values are almost the same (Table 2). The cause of the big difference in ΔE_{int} values is the drop in magnitude observed for the ΔE_{elstat} term in the $[Fe^{II}(\mathbf{bpp^X})_2]^{2+}$ family vs. the $[Fe^{II}(\boldsymbol{L^{azine}})_2(NCBH_3)_2]$ family.

This is due to the fact that the two BF_4^- (or two PF_6^-) anions are not directly bonded at the iron(II) ion in $[Fe^{II}(\mathbf{bpp^X})_2]^{2+}$; whereas the two $NCBH_3^-$ anions are directly bonded to the iron(II) ion in $[Fe^{II}(\boldsymbol{L^{azine}})_2(NCBH_3)_2]$ (Table 2).[8b] Finally, it should be noted that the ratio between ionic and covalent contributions (ΔE_{elstat}:ΔE_{orb} ratio) is important in describing the bonding between fragments.[30] For the $[Fe(\mathbf{bpp^H})_2]^{2+}$ complex the ionic: covalent ratio becomes more ionic on going from *LS* (44:55) to *HS* (50:47). This is very different from the $[Fe(\boldsymbol{L^{pyridine}})_2(NCBH_3)_2]$ complex where the *ionic* bonding is already dominating in the *LS* state (*ΔE_{elstat}:ΔE_{orb}, 55:45*), and this further increases in the *HS* state (*65:35*) (Table 2).[20] In conclusion, *EDA* analysis of these families of complexes, which feature very different types of coordination environments, is shown to correctly incorporate

Table 2. Range of ΔE_{int}, ΔE_{elstat}, and ΔE_{orb} values obtained from EDA analysis, in both HS and *LS* spin states (using fragmentation **5e**), of the sixteen $[Fe^{II}(\mathbf{bpp^X})_2]^{2+}$ complexes, compared with those previously obtained for five $[Fe^{II}(\boldsymbol{L^{azine}})_2(NCBH_3)_2]$ complexes:[20] all energies are reported in kcal/mol.

	State	ΔE_{int}	ΔE_{elstat}	ΔE_{orb}
$[Fe^{II}(\mathbf{bpp^X})_2]^{2+}$	*LS*	−250/−200	−415/−365 (~45%)	−510/−500 (~55%)
	HS	−120/−70	−330/−290 (~55%)	−315/−295 (~45%)
$[Fe^{II}(\boldsymbol{L^{azine}})_2(NCBH_3)_2]$[20]	*LS*	−530/−500	−635/−620 (~55%)	−520/−500 (~45%)
	HS	−385/−370	−585/−570 (~65%)	−330/−325 (~35%)
$\mathbf{bpp^H}$ vs. $\boldsymbol{L^{pyridine}}$	*LS*	−53%/−60%	−35%	−0.5%
	HS	−59%/−81%	−40%	−5%

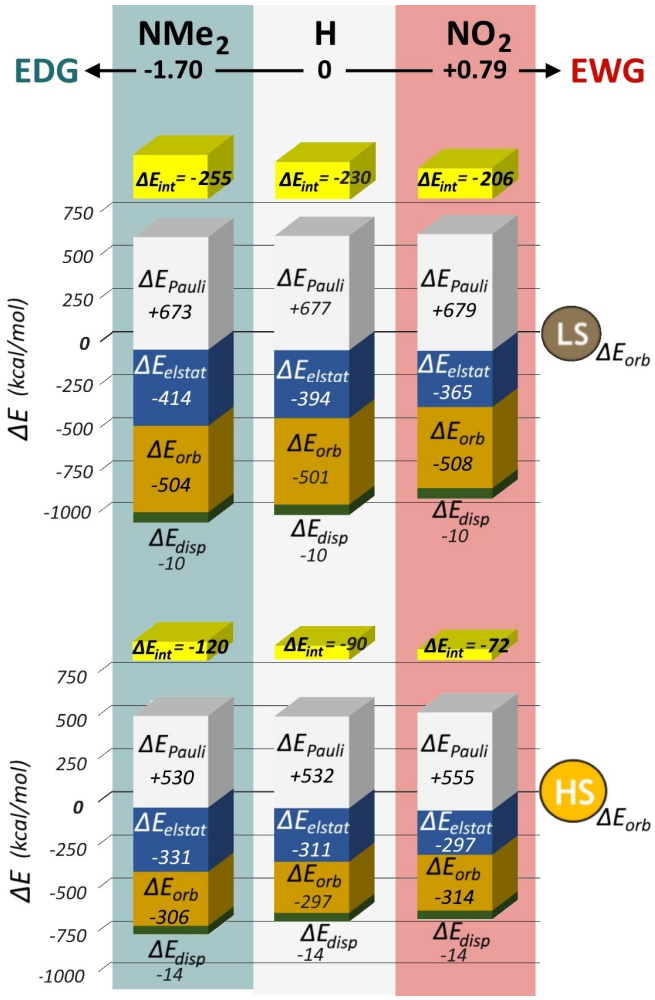

Figure 2. Results of EDA analysis of three representative $[Fe^{II}(\mathbf{bpp}^{X})_2]^{2+}$ complexes: **X** = **NMe$_2$** (left), **X** = **H** (center) and **X** = **NO$_2$** (right), in the *LS* (top) vs. *HS* (bottom) state (using fragmentation **5e**[20]). For each spin state the pair of bar graphs shows the four components of ΔE_{int} (see Equation (1); only ΔE_{Pauli} is positive) and the sum of them, ΔE_{int} (yellow).

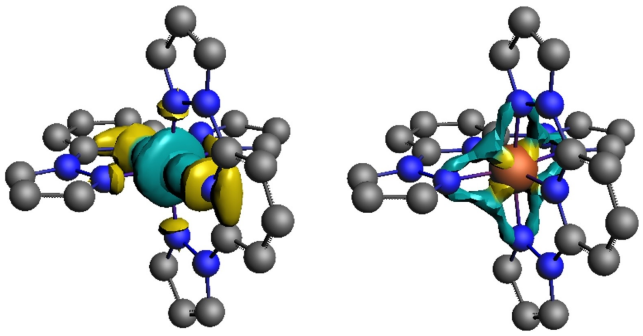

Figure 3. Example of $\mathbf{M}(d_{z2})\leftarrow\mathbf{L}_6(MO)$ σ-donation (left) and $\mathbf{M}(d_{xy})\rightarrow\mathbf{L}_6(MO)$ π-backdonation (right) in *LS* $[Fe(\mathbf{bpp}^{H})_2]^{2+}$. The direction of the charge flow is yellow→turquoise (cut-off: $\rho > 0.003$ e$^-$). A complete description of each engaged bond obtained by EDA-NOCV analysis is reported in Figures S5–S10.

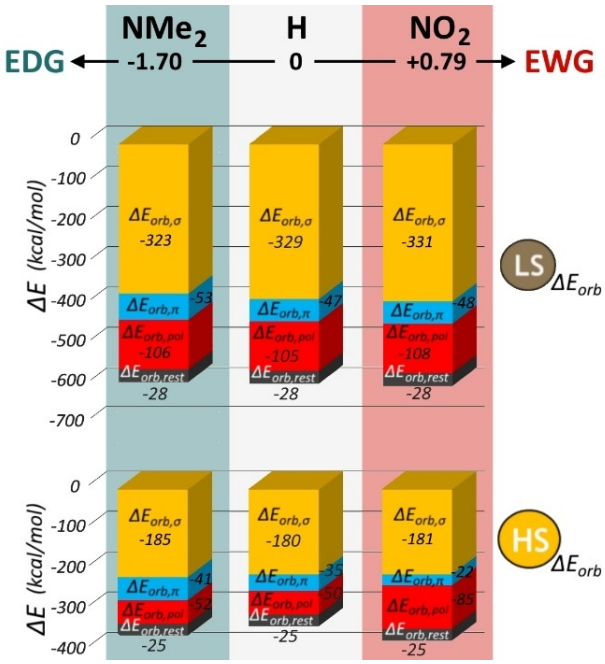

Figure 4. Results of NOCV decomposition of ΔE_{orb} of three representative $[Fe(\mathbf{bpp}^{X})_2]^{2+}$ complexes: **X** = **NMe$_2$** (left), **X** = **H** (center) and **X** = **NO$_2$** (right), in the *LS* (top) vs. *HS* (bottom) state (using fragmentation **5b**[20]). For each spin state the bar graph shows the four components of ΔE_{orb} (see Equation (2)).

details of the change in nature of the coordinative bond, regardless of the origin of the change.

NOCV analysis of the effects of X on Fe-N σ- and π-bonding in $[Fe(\mathbf{bpp}^{X})_2]^{2+}$ (LS and HS)

The full *NOCV* results obtained using the previously optimised fragmentation **5b**[20] are reported in Tables S5–S6, with selected data shown and discussed in the following sections. From the breakdown of the ΔE_{orb} term, the nine **M**+**L$_6$** bonding interactions (described by Hoffman theory[28]) can be identified by visual inspection and quantitatively assessed (Figure S1): six σ- ($\Delta E_{orb,\sigma}$), and three π-contributions ($\Delta E_{orb,\pi}$) to the **ML$_6$** interactions are sought (Figure 3 and Figure 4, Tables 3, S5–S6).

For both spin states of the sixteen complexes, the $\Delta E_{orb,\sigma}(s,p_x,p_y,p_z)$ contribution remains constant as **X** varies (Figures S5–S10). For all sixteen *LS* $[Fe(\mathbf{bpp}^{X})_2]^{2+}$ complexes, the six σ-bonds ($\Delta E_{orb,\sigma}$) account for about 85% of the $\Delta E_{orb,\sigma+\pi}$ contribution to **M**–**L** bonding, leaving only 15% of the stabilisation energy to come from the three π-bonds. The same is observed for all sixteen *HS* $[Fe^{II}(\mathbf{bpp}^{X})_2]^{2+}$ complexes ($\Delta E_{orb,\sigma}$:$\Delta E_{orb,\pi}$ = *85:15*; Tables 3 and S5–S6). In the *LS* state the overall σ-strength is mostly due to the two **M**→**L** σ-bonds formed by the $Fe^{II}(d_{z2})$ and $Fe^{II}(d_{x2-y2})$ orbitals ($\Delta E_i < -100$ kcal/mol; $v_i > 0.90$; Figure 3 (left) and Figures S5–S7).

In the sixteen *HS* $[Fe^{II}(\mathbf{bpp}^{X})_2]^{2+}$ complexes in which these two e_g anti-bonding orbitals are half-occupied, not empty, the $\Delta E_{orb,\sigma}$ stabilisation energy drops by 55% relative to the analogous *LS* state complex (Tables 3 and S5–S6). In compar-

Table 3. NOCV results (frag. **5b**) for the sixteen *LS* and *HS* $[Fe^{II}(\mathbf{bpp^X})_2]^{2+}$ complexes: all energies are reported in kcal/mol. Results are presented in order of increasing Hammett parameter (σ_p^+). *Hammett values estimated in this study. $T_{1/2}$ values for 10 of these complexes were obtained in acetone whereas the 6 marked with † were obtained in nitromethane.

X	$T_{1/2}$	σ_p^+	State	$\Delta E_{orb,\sigma+\pi}$	$\Delta E_{orb,\sigma}$	$\Delta E_{orb,\pi}$
NMe_2	HS	−1.70	*LS*	−378.5	−323.2	−52.5
			HS	−167.7	−142.1	−25.5
NH_2	HS	−1.30	*LS*	−374.8	−324.6	−50.1
			HS	−161.9	−135.8	−26.0
OH	164	−0.92	*LS*	−374.6	−325.9	−48.4
			HS	−168.9	−145.6	−23.3
OMe	158	−0.78	*LS*	−376.1	−326.4	−49.6
			HS	−156.3	−130.9	−25.3
SMe	194	−0.60	*LS*	−378.5	−326.1	−52.4
			HS	−165.9	−141.7	−24.1
Me	216	−0.31	*LS*	−376.2	−327.7	−48.2
			HS	−170.6	−147.4	−23.1
F	215	−0.31	*LS*	−374.4	−326.7	−48.5
			HS	−169.2	−142.4	−26.7
SH	246	−0.03	*LS*	−378.6	−327.6	−51.0
			HS	−170.2	−145.9	−24.3
H	248	0.00	*LS*	−376.0	−328.7	−47.3
			HS	−168.9	−142.3	−26.6
Cl	226	+0.11	*LS*	−376.9	−327.9	−49.0
			HS	−169.1	−145.7	−23.3
I	236	+0.14	*LS*	−378.9	−328.5	−50.4
			HS	−169.7	−142.8	−26.8
Br	234	+0.15	*LS*	−377.6	−327.9	−49.6
			HS	−169.7	−142.9	−26.8
CO_2H	281	+0.42	*LS*	−379.7	−331.1	−48.5
			HS	−171.7	−148.3	−23.3
NO_2	309	+0.79	*LS*	−379.7	−331.8	−48.8
			HS	−171.5	−147.7	−23.7
SOMe*	284	+0.25*	*LS*	−375.8	−328.5	−49.7
			HS	−165.2	−142.5	−22.6
SO_2Me*	294	+0.54*	*LS*	−378.2	−330.3	−47.8
			HS	−170.1	−147.7	−22.9

ison, in the *LS* $[Fe(\boldsymbol{L^{azine}})_2(NCBH_3)_2]$ complexes the six σ-bonds ($\Delta E_{orb,\sigma}$) account for even more, about 92%, of the $\Delta E_{orb,\sigma+\pi}$, the only exception for $\boldsymbol{L^{azine}}=\boldsymbol{L^{pyrdt}}$ were the σ-contribution drops to 84%; this is very likely due to a mixing between the σ- and π-contribution.[20] As well, for *HS* $[Fe^{II}(\boldsymbol{L^{azine}})_2(NCBH_3)_2]$ complexes, an even more inhomogeneity between $\Delta E_{orb,\sigma}$ and $\Delta E_{orb,\pi}$ is observed ($\Delta E_{orb,\sigma}$:$\Delta E_{orb,\pi}=98:2$).

The three π-acceptor **M**→**L** bonds are composed by two stronger degenerate π-bonds involving the $Fe^{II}(d_{z2})$ and $Fe^{II}(d_{x2-y2})$ orbitals (Figures S5–S10), and a weaker π-bond involving the $Fe^{II}(d_{xy})$ orbital (Figures S5–S10). For *LS* $[Fe^{II}(\mathbf{bpp^X})_2]^{2+}$, these three π(**M**→$\mathbf{L_6}$) interactions (slightly bonding MOs) contribute −47 kcal/mol. For *HS* $[Fe^{II}(\mathbf{bpp^X})_2]^{2+}$ these three π(**M**→$\mathbf{L_6}$) bonds contribute only −25 kcal/mol due to the *SCO* from *LS*→*HS* reducing the population of the t_{2g}-like orbitals, i.e. π-backdonation reduction. Overall, on *LS*→*HS*, stabilisation by $\Delta E_{orb,\pi}$ drops by about 40% and the overall $\Delta E_{orb,\sigma+\pi}$ drops by about 50%. In comparison, for the $[Fe(\boldsymbol{L^{azine}})_2(NCBH_3)_2]$ complexes, the $\Delta E_{orb,\sigma}$ term drops by about 50%, $\Delta E_{orb,\pi}$ drops by about 90%, and the overall $\Delta E_{orb,\sigma+\pi}$ drops by about 60%.

EDA-NOCV analysis: Correlations with σ_p^+(X)

For the *LS* $[Fe^{II}(\mathbf{bpp^X})_2]^{2+}$ family, when the Hammett constant σ_p^+(**X**) changes from **EDG** (**X**=$\mathbf{NMe_2}$) to **EWG** (**X**=$\mathbf{NO_2}$), a strong correlation is observed with $\Delta E_{orb,\sigma}$ ($R^2=0.88$, Figure 5a), a poor correlation is observed with $\Delta E_{orb,\pi}$ ($R^2=0.31$, Figure 5b), and a weak correlation is observed with the overall $\Delta E_{orb,\sigma+\pi}$ ($R^2=0.43$, Figure 5c). No correlations are observed for the *HS* $[Fe(\mathbf{bpp^X})_2]^{2+}$ complexes: σ_p^+(**X**) vs. $\Delta E_{orb,\sigma}$ ($R^2=0.30$, Figure S17); $\Delta E_{orb,\pi}$ ($R^2=0.01$, Figure S18); $\Delta E_{orb,\sigma+\pi}$ ($R^2=0.34$, Figure S19). Compared to the previous studies[8b] the effects of **X** on π-backdonation ($\Delta E_{orb,\pi}$) in this *LS* $[Fe(\mathbf{bpp^X})_2]^{2+}$ family are less linear and predictable than for the σ-donation term $\Delta E_{orb,\sigma}$. $\Delta E_{orb,\pi}$ shows a weak and opposite trend with the Hammett constant σ_p^+(**X**).

It is important to note that this divergence is not linked with the employed level of theory, as both studies employed the same *DFT* theory. Herein, as **X** varied as **EDG**→**EWG** (−1.70→+0.79), a quantitative $\Delta\Delta E_{orb,\sigma}$ stabilisation of about 5 kcal/mol is observed, along with a much less significant $\Delta\Delta E_{orb,\pi}$ destabilisation of about 1.5 kcal/mol (Tables 3, S5–S6). Not surprisingly, the σ-donor properties again dominate the π-acceptor properties, with the latter playing only a secondary role in the ligand field tuning operated by the **X** substituent.

EDA-NOCV analysis: Correlations with $T_{1/2}$

Herein, *EDA-NOCV* analysis reveals that the observed $T_{1/2}$ is also in extremely good correlation with $\Delta E_{orb,\sigma}$ for *LS* $[Fe(\mathbf{bpp^X})_2]^{2+}$

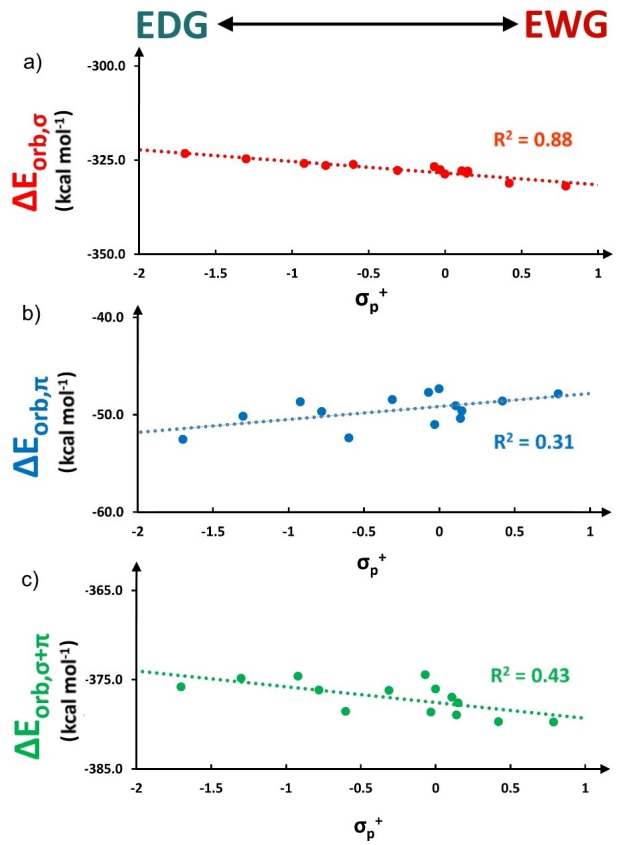

Figure 5. Correlation of σ_p^+(**X**) Hammett parameter with (a) $\Delta E_{orb,\sigma}$ ($R^2 = 0.91$); (b) $\Delta E_{orb,\pi}$ ($R^2 = 0.31$) and (c) $\Delta E_{orb,\sigma+\pi}$ ($R^2 = 0.43$) for the family of fourteen $[Fe(\mathbf{bpp^X})_2]^{2+}$ complexes (**X** = **SOMe**, **SO_2Me** are absent as σ_p^+(**X**) is not available from literature).

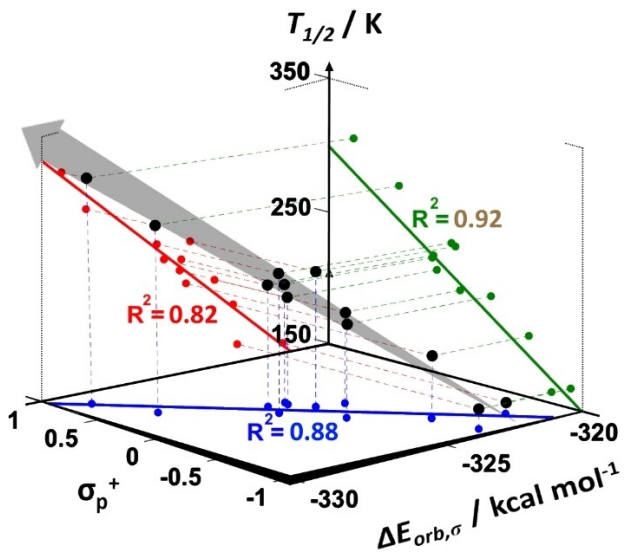

Figure 6. Three strong pairwise correlations (blue, red and green lines), and a cross-correlation (black dots; grey arrow is only a guide to the eye) between the ligand donation properties ($\Delta E_{orb,\sigma}$; calculated by EDA-NOCV for the *LS* complexes using fragmentation **5b**), the Hammett constant of **X** (σ_p^+), and the switching temperature ($T_{1/2}$) for the twelve SCO-active complexes for which σ_p^+(**X**) is known in this family of $[Fe^{II}(\mathbf{bpp^X})_2]^{2+}$ complexes (**X** = **SOMe**, **SO_2Me**, **NH_2**, **NMe_2** are absent, as σ_p^+(**X**) is not known for the first two, and the last two remain *HS*).

(Figure 6, red line, $R^2 = 0.82$ and Figure S11). On the other hand, $T_{1/2}$ does not correlate with $\Delta E_{orb,\pi}$ ($R^2 = 0.09$ Figure S12), and only very weakly correlates with $\Delta E_{orb,\sigma+\pi}$ ($R^2 = 0.48$ Figure S13). It should be recalled (see above) that for this $[Fe^{II}(\mathbf{bpp^X})_2]^{2+}$ family, $\Delta E_{orb,\sigma}$ provides 85% of the overall bonding stabilisation ($\Delta E_{orb,\sigma+\pi}$) so it is likely to dominate over changes in $\Delta E_{orb,\pi}$. In contrast, for the *HS* $[Fe(\mathbf{bpp^X})_2]^{2+}$ complexes none of the $\Delta E_{orb,i}$ terms ($i = \sigma$, π, $\sigma+\pi$) shows a promising correlation with the $T_{1/2}$ values: $\Delta E_{orb,\sigma}$ ($R^2 = 0.36$, Figure S14), $\Delta E_{orb,\pi}$ ($R^2 = 0.07$, Figure S15) and $\Delta E_{orb,\sigma+\pi}$ ($R^2 = 0.31$, Figure S16).

Therefore, these EDA-NOCV results indicate that the *LS* state is the key spin state, as it is the one for which the electronic effect of **X** on the bonding properties of the $[Fe^{II}(\mathbf{bpp^X})_2]^{2+}$ complex can be observed, through the cross-correlation of $\Delta E_{orb,\sigma}$ vs. $T_{1/2}$ (Figure 6, red line, $R^2 = 0.82$) and $\Delta E_{orb,\sigma}$ vs. σ_p^+ (Figure 6, blue line, $R^2 = 0.88$) and $T_{1/2}$ vs. σ_p^+ (Figure 6, green line, $R^2 = 0.92$).[8b]

However, the finding herein that in *LS* $[Fe^{II}(\mathbf{bpp^X})_2]^{2+}$ only $\Delta E_{orb,\sigma}$, not $\Delta E_{orb,\pi}$ or $\Delta E_{orb,\sigma+\pi}$, correlates with $T_{1/2}$ is not consistent with either (i) the intuitive rationale of the **M–L** bonding provided by Deeth, Halcrow and co-workers[8b] that **M→L** π-backbonding dominates the tuning by **X**; or (ii) the finding observed for the $[Fe^{II}(\boldsymbol{L^{azine}})_2(NCBH_3)_2]^{2+}$ family of a strong correlation for $\Delta E_{orb,\sigma+\pi}$ vs. $T_{1/2}$ ($R^2 = 0.99$) and weak correlations for $\Delta E_{orb,\sigma}$ vs. $T_{1/2}$ ($R^2 = 0.76$), $\Delta E_{orb,\pi}$ vs. $T_{1/2}$ ($R^2 = 0.88$).[20]

For issue (i), a deeper comparison of Deeth, Halcrow and co-workers[8b] finding vs. the present finding will be discussed shortly. For issue (ii), a deeper comparison of the *EDA-NOCV* results for the $[Fe^{II}(\mathbf{bpp^X})_2]^{2+}$ (**X** substituent in dicationic complex) and $[Fe^{II}(\boldsymbol{L^{azine}})_2(NCBH_3)_2]^{2+}$ (**CH/N** replacement in neutral complex) families[20] is too early at this stage as these are the only two *SCO* families studied using *EDA-NOCV* to date: investigations of more such families are required and indeed warranted.

The results obtained on the *SCO* families under study also indicate that *EDA-NOCV* analysis works much better when the number of unpaired electrons is zero (diamagnetic) i.e. for *LS* (better than *HS*). This is a consequence of using DFT as the main theoretical investigation tool in the first steps of the *EDA-NOCV* analysis, along with having a d^6 ion, as Fe^{II}, instead of using a (computationally prohibitively expensive) multi-reference approach to capture and evaluate all relevant microstates. Being intrinsically a mono-determinantal approach, DFT cannot correctly capture static correlation effects. Thus, the closed-shell *LS* Fe^{II} system can be correctly described while the open shell HS Fe^{II} system is less well described and hence is less reliable. Moreover, as the *LS* state is the most stable species at 0 K, prediction of temperature effects for it is inherently limited. Conversely, temperature effects are important for the *HS* state, but cannot be explicitly considered unless more time-consuming DFT-based ab-initio molecular dynamic (*AIMD*) calculations are used.

EDA-NOCV analysis: Correlations with δN_A

Finally, NOCV results are explored from another perspective, not yet explicitly discussed in this study. This follows from an approach first proposed by Brooker and co-workers in 2009,[31a] then followed up in 2017,[13] and further extended in 2021 to 5 families (42 complexes),[31b] in which the ^{15}N NMR chemical shift (δN_A) of the coordinating nitrogen N_A of the free ligand (easy to measure or calculate) provides a quantitative report on an N-donor ligand that has been shown to correlate well with the observed $T_{1/2}$ for the corresponding complex, in families of closely related complexes, including the **bpp^X** family of interest herein.[32]

Herein, the calculated δN_A of the **bpp^X** ligands is shown to correlate with one of the NOCV results, establishing a correlation between the properties of the **bpp^X** ligand before (free **bpp^X** ligand) and after coordinating the Fe^{II} ion ($[Fe^{II}(\mathbf{bpp^X})_2]^{2+}$ complex).

For *LS* $[Fe^{II}(\mathbf{bpp^X})_2]^{2+}$, δN_A shows an extremely good correlation with $\Delta E_{orb,\sigma}$ ($R^2 = 0.95$, Figures 7a), but only a very weak correlation with $\Delta E_{orb,\pi}$ ($R^2 = 0.39$, Figure 7b) or $\Delta E_{orb,\sigma+\pi}$ ($R^2 = 0.23$, Figure 7c).[13] In contrast, for *HS* $[Fe^{II}(\mathbf{bpp^X})_2]^{2+}$, no correlations are observed for δN_A with any $\Delta E_{orb,i}$ ($i = \sigma; \pi; \sigma+\pi$) term: $\Delta E_{orb,\sigma}$ ($R^2 = 0.35$, Figures S20), $\Delta E_{orb,\pi}$ ($R^2 = 0.04$, Figures S21) and $\Delta E_{orb,\sigma+\pi}$ ($R^2 = 0.30$, Figures S22).

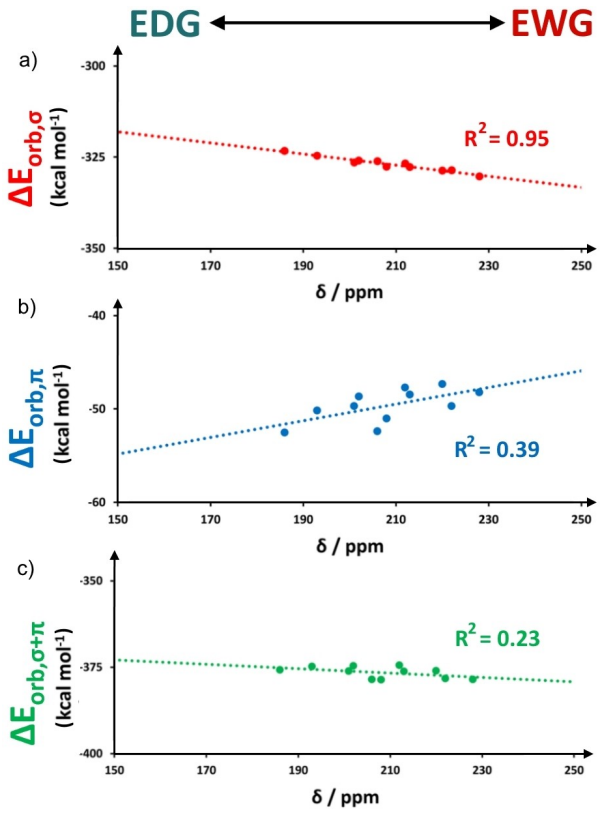

Figure 7. (a) Strong correlation ($R^2 = 0.95$) of $\Delta E_{orb,\sigma}$ with pyridine nitrogen NMR chemical shift δN_A in the family of sixteen *LS* $[Fe^{II}(\mathbf{bpp^X})_2]^{2+}$ complexes.[13] (b) Weak correlation ($R^2 = 0.39$) of $\Delta E_{orb,\pi}$ with δN_A in the family of sixteen *LS* $[Fe^{II}(\mathbf{bpp^X})_2]^{2+}$ complexes. (c) Weak correlation ($R^2 = 0.23$) of $\Delta E_{orb,\sigma+\pi}$ with δN_A in the family of sixteen *LS* $[Fe^{II}(\mathbf{bpp^X})_2]^{2+}$ complexes.

This is in full agreement with all of the findings discussed previously: the **X** substituent, the effect of which can be quantified through use of $\sigma_p^+(\mathbf{X})$, operates as a tuner of the coordinating nitrogen ligand field strength, by enriching or impoverishing the electron density, which in turn is reflected in the chemical shift, δN_A. This tweak of the nitrogen electron densities is intimately entangled with the ligand σ-donating properties ($\Delta E_{orb,\sigma}$) of the, enthalpically most stable, *LS* state that, finally, leads to an increase in the experimental $T_{1/2}$.

Mulliken population analysis

The *EDA-NOCV* results just reported project a different interpretation of the experimental results than those proposed by Deeth, Halcrow et al. in 2016.[8b] They concluded that the dominant effect of **X** changing **EDG→EWG** was increased **M→L** π-backdonation, which increased the ligand field splitting (Δ_O) and the observed solution $T_{1/2}$ values. In contrast, the above quantitative *EDA-NOCV* analysis indicates, rather counter-intuitively at first glance, that as **X** changes as **EDG→EWG**, the dominant effect is increased σ-donation **M←L**, and hence increased ligand field splitting and observed solution $T_{1/2}$ values (Figure 8).

To try to understand how **X** changing **EDG→EWG** could increase the ability of the N-donor to act as a stronger σ-donor to Fe^{II}, here the associated changes in the population of the key atomic orbitals (*AOs*) of the coordinating nitrogen, $\Delta N_A(AO)$, when the **X** substituent changes from **EDG** ($\mathbf{NMe_2}$, $\sigma_p^+ = -1.70$) to **EWG** ($\mathbf{NO_2}$, $\sigma_p^+ = +0.79$) are probed by looking at the Mulliken charges, $N_A(AO)$, for each atomic orbital,[22] as these provide a simple electronic population analysis. This investigation was performed on the relaxed *trans*-geometry of the free ligands, optimised using the same basis set employed for the related iron(II) complexes. It is worth mentioning that the observed trends are fully consistent with those obtained for the *cis*-geometry of these ligands, which is closer to the coordination geometry but is less energetically stable (Tables S7, S9).[13] Furthermore, it is important to note that the effects of varying **X**, which is *para* to the pyridine ring N donor atom (N_A), are much greater on N_A than on the coordinating nitrogen (N_{pyzl}) of the relatively remotely attached pyrazolyl ring, and, most importantly, the latter reveals the same trend as N_A does with $\sigma_p^+(\mathbf{X})$ (Figure S4, Tables S10–S11). Hence, as Deeth, Halcrow and co-workers also did,[8b] it is reasonable that the following discussion focuses attention only on the effect of varying **X** on N_A.

Examining the population of the individual valence orbitals on N_A uncovers information otherwise lost when only the overall electron density is considered, as is case when looking at the overall atomic charge ($\rho(N_A)$)[10a] or at the ^{15}N NMR chemical shift, $\delta(N_A$ (Figures S26 and S32).[13]

Mulliken charges were therefore calculated for each valence orbital on the N_A-donor atom (s, p_y, p_x, p_z), as the Hammett parameter of **X** in the ligand was changed (**EDG→EWG**, Figures S27–S30). The hybridised sp^2 is also reported vs. $\sigma_p^+(\mathbf{X})$ (Figure S31, with the electronic population taken as the average

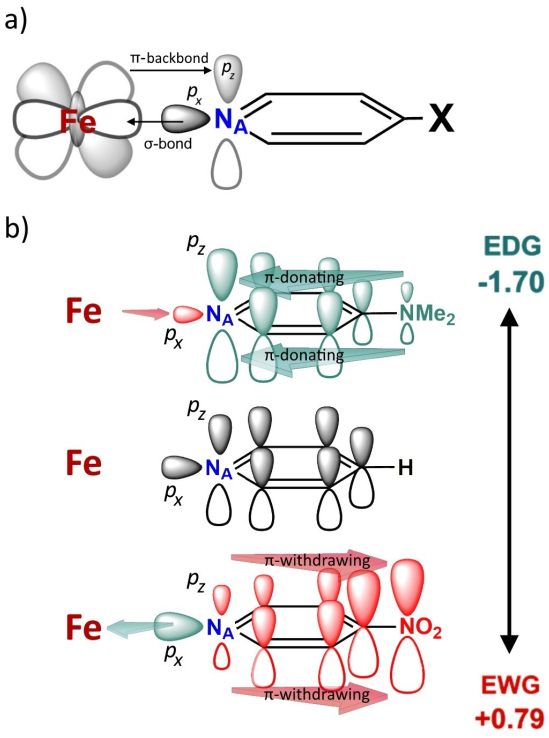

Figure 8. (a) Simplified representation of the atomic orbitals of Fe^{II} and the coordinating N_A nitrogen in the Fe–N bonding for described Mulliken population analysis. (b) Representation of the $N_A(AOs)$ of the pyridyl ring in the referenced $[Fe^{II}(\mathbf{bpp^{H}})_2]^{2+}$ complex (centre) and at the substituted ligands at the ending of the Hammett scale ($[Fe^{II}(\mathbf{bpp^{NMe2}})_2]^{2+}$, $\sigma_p^+ = -1.70$ (top); $[Fe^{II}(\mathbf{bpp^{NO2}})_2]^{2+}$, $\sigma_p^+ = +0.79$ (bottom). Arrows describe directionality of the resonance effects on the $N_A(p_z)$: toward the N_A for $[Fe^{II}(\mathbf{bpp^{NMe2}})_2]^{2+}$ and away from the N_A for $[Fe^{II}(\mathbf{bpp^{NO2}})_2]^{2+}$. The effect is complementary on the $N_A(p_x)$: enriching for $N_A(p_x)$ in $[Fe^{II}(\mathbf{bpp^{NMe2}})_2]^{2+}$ and impoverishing for $N_A(p_x)$ in $[Fe^{II}(\mathbf{bpp^{NO2}})_2]^{2+}$.

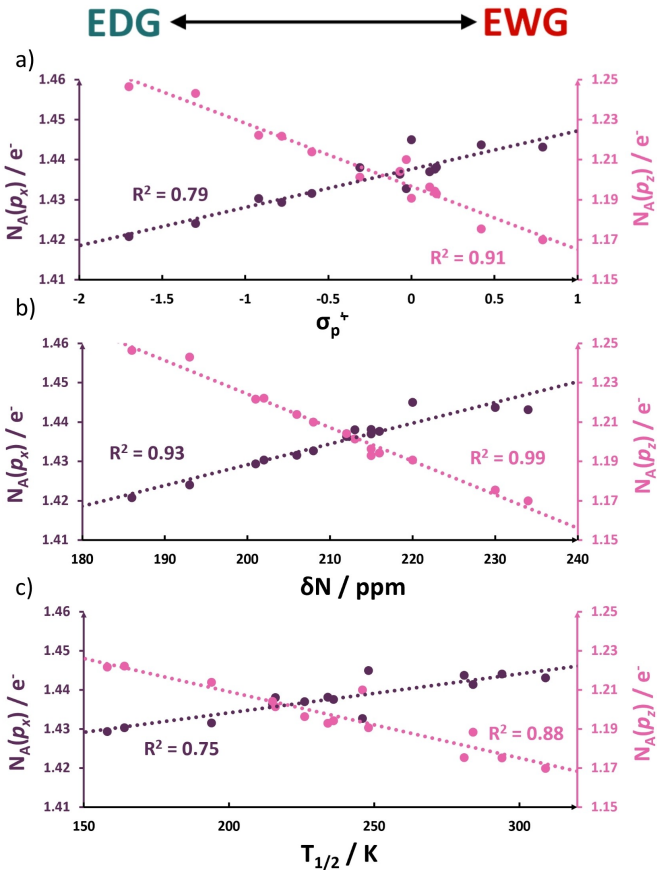

Figure 9. (a) Reported trends for the Mulliken populations $N_A(p_x)$ and $N_A(p_z)$ vs. $\sigma_p^+(\mathbf{X})$ Hammett parameter. Very good correlation is observed for $N_A(p_x)$ vs. $\sigma_p^+(\mathbf{X})$ (purple line, $R^2 = 0.79$) and an extremely good correlation for $N_A(p_z)$ vs. $\sigma_p^+(\mathbf{X})$ (pink line, $R^2 = 0.91$). (b) Reported trends for the Mulliken populations $N_A(p_x)$ and $N_A(p_z)$ vs. δN_A chemical shift. Extremely good correlation are observed for both $N_A(p_x)$ vs. δN_A (purple line, $R^2 = 0.93$) and for $N_A(p_z)$ vs. δN_A (pink line, $R^2 = 0.99$). (c) Reported trends for the Mulliken populations $N_A(p_x)$ and $N_A(p_z)$ vs. experimental $T_{1/2}$. Very good correlation is observed for $N_A(p_x)$ vs. $T_{1/2}$ (purple line, $R^2 = 0.75$) and an extremely good correlation for $N_A(p_z)$ vs. $T_{1/2}$ (pink line, $R^2 = 0.88$).

of the *s*, p_x, p_y orbital population). In the defined framework, in which all of the Fe-pyridine moiety is contained in the *xy* plane (Figure 8), the p_z ligand orbital is responsible for accepting electron density from the metal in a π-backbonding interaction (**M→L**), while the p_x ligand orbital provides the lone-pair that establishes the σ-bond to the metal (**M←L**).

Correlations between two of the $N_A(AOs)$, $N_A(p_x)$ and $N_A(p_z)$, and $\sigma_p^+(\mathbf{X})$ are seen (Figure 9a). Specifically, as the *para*-substituent **X** changes **EDG→EWG**, the associated increase in the Hammett parameter, $\sigma_p^+(\mathbf{X})$, correlates extremely well ($R^2 =$ 0.91, pink line in Figure 9a) with electron depletion of the p_z orbital $N_A(p_z)$ and correlates well ($R^2 = 0.79$, purple line in Figure 9a) with electron accumulation in the p_x orbital $N_A(p_x)$. Overall, from **NMe_2→NO_2**, the decrease in population of the p_z orbital is $\Delta N_A(p_z) = +0.08$ e, whilst the increase in the population of the p_x orbital is more modest, $\Delta N_A(p_x) = -0.03$ e.

Therefore, whilst electronic population in $N_A(p_z)$ is decreased as the **X** substituent becomes more **EWG**, making it a better acceptor for **M→L** π backbonding, the $N_A(p_x)$ population is increased, resulting in more available electron density in the lone-pair, which facilitates stronger **M←L** σ bonding and with it an increase in $T_{1/2}$ - in alignment with the common interpretation from crystal field theory first principles.

For completeness, it should be noted that *para*-**X** substituent only has tiny effects on the $N_A(s)$ ($\Delta e^- < -0.002$, **NMe_2→NO_2**) and $N_A(p_y)$ atomic orbitals ($\Delta e^- < -0.004$, **NMe_2→NO_2**), which also results in a lack of correlations with $\sigma_p^+(\mathbf{X})$ ($R^2(N_A(s)) =$ 0.27, Figure S27 and $R^2(N_A(p_y)) = 0.02$, Figure S29). Combining these to form the $N_A(sp^2)$ hybrid orbital, the result is a good correlation with $\sigma_p^+(\mathbf{X})$ ($R^2(N_A(sp^2)) = 0.73$, Figure S31).

As the $N_A(s)$ and $N_A(p_y)$ atomic orbitals look almost unaffected by the electronic nature of the **X** substituent, it can be assumed that the $N_A(p_z)$ and $N_A(p_x)$ atomic orbitals are intimately affecting each other. For **EDG** substituents, this behavior can be explained as arising from the enrichment of π-density ($N_A(p_z)$) inducing a compensating electrostatic draining of σ-density ($N_A(p_x)$), all of which directly influences the bonding properties of the coordinated N_A atom. The opposite trend is expected for the **EWG** substituents.

In previous studies it was observed that δN_A is intimately connected with $T_{1/2}$[13] and hence also with $\sigma_p^+(\mathbf{X})$. Therefore,

herein possible relationships of δN_A with the Mulliken population analysis results are probed (Figure 9b). Unsurprisingly, the results are in full agreement with the observations just reported for $N_A(AOs)$ vs. $\sigma_p^+(X)$ trends (Figure 9a). Indeed, the correlations with $N_A(p_z)$ and $N_A(p_x)$ are even stronger when using δN_A, which has the advantages of being an easily calculated but also experimentally verifiable value for the specific ligand used, rather than using $\sigma_p^+(X)$ for the substituent used.

An excellent correlation of increasing δN_A with decreasing $N_A(p_z)$ ($R^2 = 0.99$, pink line in Figures 9b, S36) and with increasing $N_A(p_x)$ ($R^2 = 0.93$, purple line in Figures 9b, Figure S34) is observed. Again no correlation is observed for δN_A vs. $N_A(s)$ ($R^2 = 0.41$, Figure S33) or vs. $N_A(p_y)$ ($R^2 = 0.0002$), Figure S35). When combined, a very good correlation is observed for δN_A with $N_A(sp^2)$ ($R^2 = 0.93$, Figure S37). As well, very good correlations are also observed for the experimental $T_{1/2}$ vs. $N_A(p_x)$ ($R^2 = 0.88$, purple line in Figures 9c and S40) and $N_A(p_z)$ ($R^2 = 0.75$, pink line in Figures 9c and S42). Experimental $T_{1/2}$ was also tested vs. $\rho(N_A)$ ($R^2 = 0.85$, Figure S38), $N_A(s)$ ($R^2 = 0.22$, Figure S39), $N_A(p_y)$ ($R^2 = 0.03$), Figure S41), and the combined $N_A(sp^2)$ ($R^2 = 0.74$, Figure S43).

Herein, the two orbital populations $N_A(p_x)$ and $N_A(p_z)$ were also tested vs. the orbital energy terms $\Delta E_{orb,\sigma}$, $\Delta E_{orb,\pi}$ and $\Delta E_{orb,\sigma+\pi}$. (Figure 10). The $\Delta E_{orb,\sigma}$ term correlates extremely well with both $N_A(p_x)$ ($R^2 = 0.84$, Figure 10a) and $N_A(p_z)$ ($R^2 = 0.93$, Figure 10b), revealing how the variation of occupancy in these two orthogonal orbitals contributes to the σ-donating properties of the ligand.

Not surprisingly, given the poor correlations of $\Delta E_{orb,\pi}$ or $\Delta E_{orb,\sigma+\pi}$ with either the Hammett parameter $\sigma_p^+(X)$ or observed $T_{1/2}$ or calculated chemical shift δN_A (see above), poor correlations were found for $\Delta E_{orb,\pi}$ with $N_A(p_x)$ ($R^2 = 0.49$, Figure S44) or $N_A(p_z)$ ($R^2 = 0.36$, Figure S45), and for $\Delta E_{orb,\sigma+\pi}$ with $N_A(p_x)$ ($R^2 = 0.29$, Figure S46) or $N_A(p_z)$ ($R^2 = 0.46$, Figure S47).

For above findings to be useful, it is critical that they are not dependent on the specific method of charge analysis employed, so the same analysis was also performed using the Loewdin framework in the atomic charge assessment (Table S8, Figures S48-S50), and this confirmed the above findings.

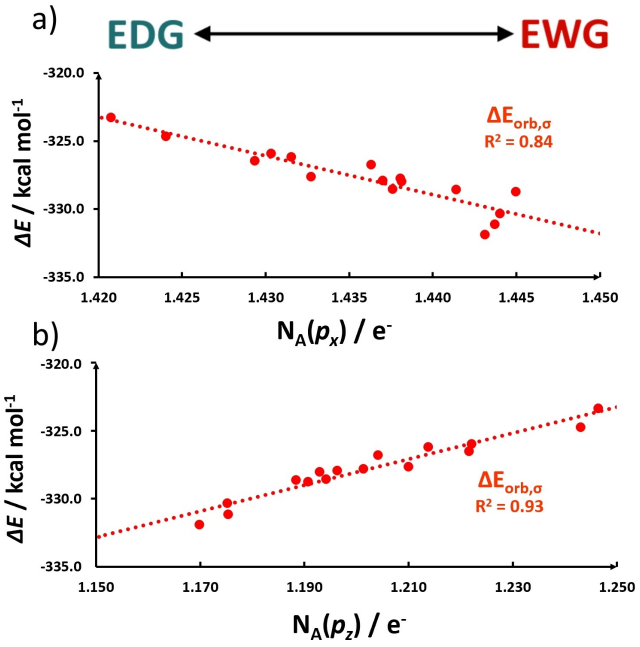

Figure 10. (a) Correlation of Mulliken p_x-electrons population $N_A(p_x)$ of the family of sixteen bpp^X ligands with the $\Delta E_{orb,\sigma}$ energetic term of the $[Fe^{II}(bpp^X)_2]^{2+}$ complex ($R^2 = 0.84$). (b) Correlation of Mulliken p_z-electrons population $N_A(p_z)$ of the family of sixteen bpp^X ligands with the $\Delta E_{orb,\sigma}$ energetic term of the $[Fe^{II}(bpp^X)_2]^{2+}$ complex ($R^2 = 0.93$).

Comparison of these results with the literature

In their landmark 2016 paper, Halcrow, Deeth and coworkers[8b] proposed an intuitively reasonable explanation, also consistent with the calculated *MO* energy levels of the $[Fe^{II}(bpp^X)_2]^{2+}$ complexes, of the effect of the *para*-**X** substituents on the $T_{1/2}$ values in this family of *SCO* active complexes: that **M**→**L** π-backdonation dominates in these **M**–**L** bonds. Hence, in the quantitative EDA-NOCV analysis of the **M**–**L** bond contributions performed herein, a correlation between $\Delta E_{orb,\pi}$ and $T_{1/2}$ was expected - but was not observed ($R^2 = 0.09$, Figure S12).

However, the proposed dominance of the **M**→**L** π-backdonation was based on the observation of a slope difference between the correlation lines for $\sigma_p^+(X)$ vs. Fe^{II} $<E(t_{2g})>$ (−0.39) and $<E(e_g)>$ (−0.32),[7b] Error bars would have helped in analysing the significance of this small difference in slope. Indeed, a larger variance is expected for Fe^{II} $E(t_{2g})$ than for Fe^{II} $E(e_g)$, so what was claimed as a "greater effect on the averaged $<E(t_{2g})>$ orbital energies than on the $<E(e_g)>$ orbitals" could be an overstatement. Also, in ref[7b] the halogen **X** substituents (four dots: **X** = **F**, **Cl**, **Br**, **I**) had to be separately grouped from all of the other electron-withdrawing **X** substituents. They behave differently to the other **X** groups, specifically they have a greater effect on the $E(e_g)$ than on the $E(t_{2g})$ *MOs*. All of these effects are accurately reflected in the present EDA-NOCV analysis, which therefore provides a coherent and detailed picture of the relative impact of **M**–**L** σ- versus π-bonding in determining the observed $T_{1/2}$, effectively refining the earlier interpretation by Halcrow, Deeth and co-workers.[8b] In support of this, the perfect agreement between our results and the ΔE(*HS-LS*) vs. $\sigma_p^+(X)$ reported in their work is revelatory.[7b]

Predicting σ_p and σ_p^+ for X = SOMe, SO_2Me

In this study, several correlations have been identified whereby the electronic tuning by **X** modifies the electron density over the coordinating nitrogen N_A and, consequently, its coordinating properties in engaging in the Fe–N bond in these sixteen $[Fe^{II}(bpp^X)_2]^{2+}$ complexes. These correlations, weight averaged by the relative R^2 values, can be employed to predict the Hammett constants for substituents **X** for which they are not known. For two out of the sixteen $[Fe^{II}(bpp^X)_2]^{2+}$ complexes, those with **X** = **SOMe** and **X** = **SO_2Me**, whilst the $\sigma_p(X)$ parameter is known, the $\sigma_p^+(X)$ parameter is not available.[5,7a]

Firstly, this approach was trialled for estimating the known σ_p(**X**) parameters,[7b] giving σ_p(**SOMe**) ≈ 0.31 vs. the literature value of 0.49, and similarly, σ_p(**SO_2Me**) ≈ 0.52 vs. the literature value of 0.72, with both predicted values lying about 0.2 units below the literature values. A general underestimation of the literature values is observed in all the explored correlations (Table S12).

Secondly, in the same way, the set of seven correlations, Equations S1–S7, identified in this study were used to predict the unknown values of σ_p^+(**X**) for **X** = **SOMe** and **X** = **SO_2Me** (Table 4, Table S13), as ≈0.25 and ≈0.54, respectively.

Finally, we note that in future studies by us and others, consideration could be given to using parameters designed for azine (and azole) derivatives,[32] in place of the Hammett parameter which arises from consideration of benzoic acid derivatives.[5]

Conclusion

Inspired by the 2016 landmark study by Deeth, Halcrow and co-workers,[8b] the effect of the *para*-substituent **X** on the electronic structure of sixteen solution *SCO* active $[Fe^{II}(\mathbf{bpp^X})_2]^{2+}$ complexes has been investigated in more depth herein, by quantifying the contributions to the **M**–**L** bonds through use of *EDA-NOCV* analysis, and then, due to the unexpected findings from that study, a Mulliken charge analysis was also conducted.

Specifically, the *EDA-NOCV* results unexpectedly revealed a strong correlation between the σ-donor strength ($\Delta E_{orb,\sigma}$) of the **bpp^X** ligand in the *LS* $[Fe^{II}(\mathbf{bpp^X})_2]^{2+}$ complex and the measured $T_{1/2}$ of the complex ($R^2 = 0.82$), but not with $\Delta E_{orb,\pi}$ or $\Delta E_{orb,\sigma+\pi}$. Furthermore, $\Delta E_{orb,\sigma}$ also correlated strongly with the ^{15}N NMR chemical shift $\delta\mathbf{N_A}$(**bpp^X**) ($R^2 = 0.95$), and with σ_p^+(**X**) ($R^2 = 0.88$).

These correlations, of $\Delta E_{orb,\sigma}$ with $T_{1/2}$, σ_p^+(**X**) and $\delta\mathbf{N_A}$, were further probed by analysis of the Mulliken charges for the $\mathbf{N_A}$ valence orbitals. Moving from **EDG** to **EWG** *para*-substituents **X**, the analysis of the Mulliken charges showed that the electron population in the $\mathbf{N_A}(p_z)$ orbital decreases (as it is delocalised in the ligand π-system towards the **X** substituent), whilst the population in the nitrogen lone pair, $\mathbf{N_A}(p_x)$, orthogonal to $\mathbf{N_A}(p_z)$, increases. An enhancement of the σ-donation ($\mathbf{Fe^{II}}\leftarrow\mathbf{N_A}$) is therefore expected, as is enhancement of the π-acceptor character ($\mathbf{Fe^{II}}\rightarrow\mathbf{N_A}$). Both of these effects lead to an increase the ligand field and hence an increase of $T_{1/2}$, as experimentally observed. The key difference from Halcrow and Deeth's intuitive finding is that the EDA-NOCV quantitative analysis indicates that the σ-donation $\mathbf{Fe^{II}}\leftarrow\mathbf{N_A}$ dominates, whereas they proposed that the π-acceptor character $\mathbf{Fe^{II}}\rightarrow\mathbf{N_A}$ dominates. Indeed, a critical look at Halcrow and Deeth's results shows a similar dependence of both σ-donation and π-acceptor for $[Fe^{II}(\mathbf{bpp^X})_2]^{2+}$, depicting a picture not too different from ours.

It is also interesting to note that the EDA-NOCV findings for the $[Fe^{II}(\mathbf{bpp^X})_2]^{2+}$ family studied herein (correlations only with $\Delta E_{orb,\sigma}$, not with $\Delta E_{orb,\sigma+\pi}$ or $\Delta E_{orb,\pi}$) differ from those found for the only other *SCO*-active family studied to date, wherein a correlation was found only with $\Delta E_{orb,\sigma+\pi}$, not $\Delta E_{orb,\sigma}$ or $\Delta E_{orb,\pi}$.[20] This might indicate that EDA-NOCV analysis may be sensitive to different coordination bond schemes (i.e. kinds of ligands), but the important point is the confirmation that excellent trends between EDA-NOCV parameters and $T_{1/2}$ values are found for the different Fe(II) families studied to date. Nevertheless, it must be borne in mind that to date these are the only two in depth studies of *SCO*-active families so it is too soon to draw conclusions from this. Rather, it is clear that further such studies are warranted.

Finally, it is also important to note that while the above EDA-NOCV analysis captures the majority of enthalpic effects, it does not account for any explicit entropic contributions. Indeed, the $T_{1/2}$ values arise from a delicate balance of very subtle effects of these two contributions, that can have drastic consequences on the SCO. Hence the future development of this approach for applications in the SCO field should also involve finding ways to evaluate if, and how, entropic contributions need to be included in the EDA-NOCV analysis when systems that are structurally very different are considered.

Computational Details

Calculations were performed using ORCA 4.1[33] and ADF (version 2018.106) code.[34] The ORCA code was used to optimise the structure of sixteen of the $[Fe^{II}(\mathbf{bpp^X})_2]^{2+}$ complexes (in both *HS* and *LS* states); the absence of negative eigenvalues for the Hessian matrix confirmed the all computed geometries are in real minima.

Firstly, using the atomic coordinates of the sixteen *LS* and sixteen *HS* $[Fe^{II}(\mathbf{bpp^X})_2]^{2+}$ complexes available from the *DFT* study at RI-BP86-D3(BJ)/def2-SVP/J + COSMO(acetone) level of theory in the paper by Deeth, Halcrow et al.,[8b] a geometry re-optimisation was performed using different RI-BP86-D3(BJ)/def2-TZVPP + CPCM level of theory:[25,35] i.e. RI = resolution of identity[35f,g] with a BP86

Table 4. Predicted values of σ_p^+(**X**) for the two **X** substituents for which this value is not reported in literature, using the correlations identified in this study with the best correlation factor, followed by the weighted average value highlighted in yellow.

		σ_p^+ *X = SOMe*	σ_p^+ *X = SO_2Me*	R^2
LS $[Fe^{II}(\mathbf{bpp^X})_2]^{2+}$	ΔE_{elstat}	0.20	0.65	0.89
	$\Delta E_{orb,\sigma}$	0.01	0.50	0.88
Exp.	$T_{1/2}$	0.53	0.64	0.92
bpp^X	$\delta^{15}N_A$	0.27	0.58	0.92
	$\rho(N_A)$	0.23	0.66	0.93
	$N_A(p_x)$	0.28	0.51	0.79
	$N_A(p_z)$	0.23	0.62	0.91
weight.av. **(σ_p^+)**		**0.25**	**0.54**	–

functional,[35c,d] with D3 dispersion correction (including BJ damping),[25] def2-TZVPP basis set,[35a] and the solvent modelled by CPCM.[35e] The same was done for the *trans* and *cis* forms of the sixteen free **bpp**^{x} ligands.

Secondly, the optimised structures of the complexes were used for the *EDA-NOCV*[27] method that combines classical *EDA*[18] with *NOCV*,[19] which were performed using the ADF2019.106 program package at the BP86-D3(BJ)/TZ2P level of theory.[34,36] It should be noted that the *EDA-NOCV* is implemented with no possibility to include any solvation model. Finally, the fully optimised geometries of the ligands were used for the Mulliken and Loewdin analyses.

Acknowledgements

We thank the University of Otago, including a Ph.D. scholarship (2017-2021) and a publishing bursary (2021) to L.B. and the INSTM consortium, fellowship (2021) to L.B. We acknowledge the 'Progetto Dipartimenti di Eccellenza 2018–2022' (ref B96C1700020008) for supporting this research. We acknowledge the contribution of the NeSI high performance computing facilities (NZ). We are grateful to the referees for their constructive comments which have enabled us to further improve this manuscript. Open access publishing facilitated by University of Otago, as part of the Wiley - University of Otago agreement via the Council of Australian University Librarians.

Conflict of Interest

The authors declare no conflict of interest.

Data Availability Statement

The data that support the findings of this study are available in the supplementary material of this article.

Keywords: M–L bonding · Hammett constant · iron(II) · spin crossover · substituent · theoretical

[1] a) M. A. Halcrow, *Chem. Soc. Rev.* **2008**, *37*, 278–289; b) E. Ruiz, *Phys. Chem. Chem. Phys.* **2014**, *16*, 14–22; c) G. Molnár, L. Salmon, W. Nicolazzi, F. Terkib, A. Bousseksou, *J. Mater. Chem. C* **2014**, *2*, 1360–1366.
[2] a) A. Tissot, *New J. Chem.* **2014**, *38*, 1840–1845; b) P. G. Lacroix, I. Malfant, J.-A. Real, V. Rodriguez, *Eur. J. Inorg. Chem.* **2013**, *2013*, 615–627; c) A. Bousseksou, L. Salmon, G. Molnar, S. Cobo in *Heat-sensitive spin-transition materials doped with one or more fluorescent agents for use as temperature sensor*, Centre National de la Recherche Scientifique C. N. R.S, France. **2011**, 54pp.
[3] A. G. Maher, G. Passard, D. K. Dogutan, R. L. Halbach, B. L. Anderson, C. J. Gagliardi, M. Taniguchi, J. S. Lindsey, D. G. Nocera, *ACS Catal.* **2017**, *7*, 3597–3606.
[4] J.-H. Yum, E. Baranoff, F. Kessler, T. Moehl, S. Ahmad, T. Bessho, A. Marchioro, E. Ghadiri, J.-E. Moser, C. Yi, M. K. Nazeeruddin, M. Grätzel, *Nat. Commun.* **2012**, *3*, 631.
[5] L. P. Hammett, *J. Am. Chem. Soc.* **1937**, *59*, 96–103.
[6] a) Y. Okamoto, H. C. Brown, *J. Org. Chem.* **1957**, *22*, 485–494; b) L. M. Stock, H. C. Brown, *Adv. Phys. Org. Chem.* **1963**, *1*, 35–154.
[7] a) L. P. Hammett, *Chem. Rev.* **1935**, *17*, 125–136; b) C. Hansch, A. Leo, R. W. Taft, *Chem. Rev.* **1991**, *91*, 165–195.
[8] a) S. Rodríguez-Jiménez, L. Bondì, M. Yang, A. L. Garden, S. Brooker, *Chem. Asian J.* **2019**, *14*, 1158–1166; b) L. J. Kershaw Cook, R. Kulmaczewski, R. Mohammed, S. Dudley, S. A. Barrett, M. A. Little, R. J. Deeth, M. A. Halcrow, *Angew. Chem. Int. Ed.* **2016**, *55*, 4327–4331; *Angew. Chem.* **2016**, *128*, 4399–4403.
[9] J. N. McPherson, R. W. Hogue, F. S. Akogun, L. Bondì, E. T. Luis, J. R. Price, A. L. Garden, S. Brooker, S. B. Colbran, *Inorg. Chem.* **2019**, *58*, 2218–2228.
[10] a) A. Kimura, T. Ishida, *ACS Omega* **2018**, *3*, 6737–6747; b) I. Prat, A. Company, T. Corona, T. Parella, X. Ribas, M. Costas, *Inorg. Chem.* **2013**, *52*, 9229–9244.
[11] a) P. Gütlich, H. A. Goodwin, *Top. Curr. Chem.* **2004**, *233*, 1–47; b) A. Hauser, *Top. Curr. Chem.* **2004**, *234*, 155–198; c) A. B. Gaspar, M. Seredyuk, *Coord. Chem. Rev.* **2014**, *268*, 41–58; d) S. Brooker, *Chem. Soc. Rev.* **2015**, *44*, 2880–2892 and front cover feature; e) J.-F. Letard, *J. Mater. Chem.* **2006**, *16*, 2550–2559; f) K. Oka, M. Azuma, W.-t. Chen, H. Yusa, A. A. Belik, E. Takayama-Muromachi, M. Mizumaki, N. Ishimatsu, N. Hiraoka, M. Tsujimoto, M. G. Tucker, J. P. Attfield, Y. Shimakawa, *J. Am. Chem. Soc.* **2010**, *132*, 9438–9443; g) M. J. Murphy, K. A. Zenere, F. Ragon, P. D. Southon, C. J. Kepert, S. M. Neville, *J. Am. Chem. Soc.* **2017**, *139*, 1330–1335; h) G. Chastanet, C. Desplanches, C. Baldé, P. Rosa, M. Marchivie, P. Guionneau, *Chem. Sq.* **2018**, *2*, 2; i) L. Bondì, S. Brooker, F. Totti, *J. Mater. Chem. C* **2021**, *9*, 14256–14268.
[12] M. A. Halcrow, I. Capel Berdiell, C. M. Pask, R. Kulmaczewski, *Inorg. Chem.* **2019**, *58*, 9811–9821.
[13] S. Rodríguez-Jiménez, M. Yang, I. Stewart, A. L. Garden, S. Brooker, *J. Am. Chem. Soc.* **2017**, *139*, 18392–18396.
[14] a) H. Phan, J. J. Hrudka, D. Igimbayeva, L. M. Lawson Daku, M. Shatruk, *J. Am. Chem. Soc.* **2017**, *139*, 6437–6447; b) K. Nakano, N. Suemura, K. Yoneda, S. Kawata, S. Kaizaki, *Dalton Trans.* **2005**, 740–743; c) J.-F. Létard, C. Carbonera, J. A. Real, S. Kawata, S. Kaizaki, *Chem. Eur. J.* **2009**, *15*, 4146–4155; d) W. Phonsri, L. Darveniza, S. Batten, K. Murray, *Inorganics* **2017**, *5*, 51; e) J. G. Park, I.-R. Jeon, T. D. Harris, *Inorg. Chem.* **2015**, *54*, 359–369; f) W. Phonsri, D. S. Macedo, K. R. Vignesh, G. Rajaraman, C. G. Davies, G. N. L. Jameson, B. Moubaraki, J. S. Ward, P. E. Kruger, G. Chastanet, K. S. Murray, *Chem. Eur. J.* **2017**, *23*, 7052–7065; g) K. Takahashi, Y. Hasegawa, R. Sakamoto, M. Nishikawa, S. Kume, E. Nishibori, H. Nishihara, *Inorg. Chem.* **2012**, *51*, 5188–5198.
[15] K. Nakano, N. Suemura, K. Yoneda, S. Kawata, S. Kaizaki, *Dalton Trans.* **2005**, 740–743.
[16] R. J. Deeth, M. Halcrow, L. Kershaw Cook, P. Raithby, *Chem. Eur. J.* **2018**, *24*, 5204–5212.
[17] a) J. M. Holland, J. A. McAllister, C. A. Kilner, M. Thornton-Pett, A. J. Bridgeman, M. A. Halcrow, *Dalton Trans.* **2002**, *2002*, 548; b) L. J. Kershaw Cook, R. Kulmaczewski, S. A. Barrett, M. A. Halcrow, *Inorg. Chem. Front.* **2015**, *2*, 662–670; c) L. J. Kershaw Cook, J. Fisher, L. P. Harding, M. A. Halcrow, *Dalton Trans.* **2015**, *44*, 9417–9425; d) R. Pritchard, C. A. Kilner, S. A. Barrett, M. A. Halcrow, *Inorg. Chim. Acta* **2009**, *362*, 4365–4371; e) R. Pritchard, H. Lazar, S. A. Barrett, C. A. Kilner, S. Asthana, C. Carbonera, J.-F. Letard, M. A. Halcrow, *Dalton Trans.* **2009**, 6656–6666.
[18] a) T. Ziegler, A. Rauk, *Inorg. Chem.* **1979**, *18*, 1755–1759; b) T. Ziegler, A. Rauk, *Inorg. Chem.* **1979**, *18*, 1558–1565.
[19] a) M. Mitoraj, A. Michalak, *J. Molec. Modeling* **2008**, *14*, 681–687; b) A. Michalak, M. Mitoraj, T. Ziegler, *J. Phys. Chem. A* **2008**, *112*, 1933–1939.
[20] L. Bondì, A. L. Garden, P. Jerabek, F. Totti, S. Brooker, *Chem. Eur. J.* **2020**, *26*, 13677–13685.
[21] a) D. C. Ashley, E. Jakubikova, *Inorg. Chem.* **2018**, *57*, 9907–9917; b) M. A. Halcrow, *Dalton Trans.* **2020**, *49*, 15560–15567.
[22] a) R. S. Mulliken, *J. Chem. Phys.* **1955**, *23*, 2343–2346; b) R. S. Mulliken, *J. Chem. Phys.* **1955**, *23*, 1833–1840.
[23] L. Zhao, M. von Hopffgarten, D. M. Andrada, G. Frenking, *Wiley Interdiscip. Rev.: Comput. Mol. Sci.* e1345.
[24] F. M. Bickelhaupt, E. J. Baerends, *Rev. Comput. Chem.* **2000**, *15*, 1–86.
[25] a) S. Grimme, J. Antony, S. Ehrlich, H. Krieg, *J. Chem. Phys.* **2010**, *132*, 154104; b) S. Grimme, S. Ehrlich, L. Goerigk, *J. Comput. Chem.* **2011**, *32*, 1456–1465.
[26] a) M. P. Mitoraj, A. Michalak, T. Ziegler, *J. Chem. Theory Comput.* **2009**, *5*, 962–975; b) M. Mitoraj, A. Michalak, *J. Molec. Model.* **2007**, *13*, 347–355.
[27] a) S. Lin, C. S. Diercks, Y.-B. Zhang, N. Kornienko, E. M. Nichols, Y. Zhao, A. R. Paris, D. Kim, P. Yang, O. M. Yaghi, *Science* **2015**, *349*, 1208–1213; b) G. Frenking, S. Shaik, *The Chemical Bond: Chemical Bonding Across the Periodic Table*, John Wiley & Sons, **2014**.
[28] T. A. Albright, J. K. Burdett, M.-H. Whangbo, *Orbital interactions in chemistry*, John Wiley & Sons, **2013**.

[29] M. Cossi, N. Rega, G. Scalmani, V. Barone, *J. Comput. Chem.* **2003**, *24*, 669–681.
[30] G. Frenking, *J. Organomet. Chem.* **2001**, *635*, 9–23.
[31] a) J. A. Kitchen, N. G. White, M. Boyd, B. Moubaraki, K. S. Murray, P. D. W. Boyd, S. Brooker, *Inorg. Chem.* **2009**, *48*, 6670–6679; b) L. Bondì, S. Rodríguez-Jiménez, H. L. C. Feltham, A. L. Garden, S. Brooker, *Inorg. Chem. Front.* **2021**, *8*, 4846–4857.
[32] A. Mazurek, J. C. Dobrowolski, *J. Org. Chem.* **2012**, *77*, 2608–2618.
[33] F. Neese, *WIREs Comput. Mol. Sci.* **2018**, *8*, e1327.
[34] G. t. Te Velde, F. M. Bickelhaupt, E. J. Baerends, C. Fonseca Guerra, S. J. van Gisbergen, J. G. Snijders, T. Ziegler, *J. Comput. Chem.* **2001**, *22*, 931–967.
[35] a) F. Weigend, R. Ahlrichs, *Phys. Chem. Chem. Phys.* **2005**, *7*, 3297–3305; b) F. Weigend, *Phys. Chem. Chem. Phys.* **2006**, *8*, 1057–1065; c) A. D. Becke, *Phys. Rev. A* **1988**, *38*, 3098–3100; d) J. P. Perdew, W. Yue, *Phys. Rev. B* **1986**, *33*, 8800–8802; e) Y. Takano, K. N. Houk, *J. Chem. Theory Comput.* **2005**, *1*, 70–77; f) O. Vahtras, J. Almlöf, M. W. Feyereisen, *Chem. Phys. Lett.* **1993**, *213*, 514–518; g) F. Weigend, M. Häser, *Theor. Chem. Acc.* **1997**, *97*, 331–340.
[36] E. Van Lenthe, E. J. Baerends, *J. Comput. Chem.* **2003**, *24*, 1142–1156.

Manuscript received: December 2, 2021
Accepted manuscript online: February 27, 2022
Version of record online: March 21, 2022